



# High-sensitivity 308.6-nm laser absorption diagnostic optimized for OH measurement in shock tube combustion studies

Shengkai Wang<sup>1</sup> · Ronald K. Hanson<sup>1</sup>

Received: 16 October 2017 / Accepted: 24 January 2018 / Published online: 8 February 2018  
© Springer-Verlag GmbH Germany, part of Springer Nature 2018

## Abstract

We report the development of a high-sensitivity laser absorption diagnostic optimized for measurement of the hydroxyl radical (OH) at temperatures relevant to combustion studies, and demonstrated here in shock tube experiments. This diagnostic utilizes a narrow-linewidth CW UV laser that is tunable over the  $A^2\Sigma - X^2\Pi(0,0)$  band of the OH rovibronic transitions. First, we identified the strongest absorption transition of OH, over the current temperature range of interest, to be the  $Q_1(5)$  transition near 308.61 nm. We then measured the OH absorption coefficients behind reflected shock waves over temperatures of 1656–2993 K and pressures of 0.88–4.09 atm, and determined the pressure-broadening and pressure-shifting coefficients in argon bath gas. Compared to the previous diagnostic targeting the OH  $R_1(5)$  transition, the current diagnostic has approximately 2.2 times the sensitivity. Finally, we demonstrated the excellent sensitivity of the current OH diagnostic in a set of highly-diluted  $C_3H_8$  oxidation experiments in a shock tube, where a  $1 - \sigma$  detection limit of less than 0.15 ppm OH was successfully achieved.

## 1 Introduction

As the primary carrier of chain branching and propagation reactions, the hydroxyl radical, OH, is one of the most important intermediate species in hydrogen and hydrocarbon combustion chemistry. Consequently, there is a strong need in the combustion community for the ability to accurately measure OH at elevated temperatures. Previous researchers have demonstrated the use of laser-induced fluorescence [1–7], emission [8–13] and absorption [14–25] spectroscopy, at both UV [1–8, 10–13, 16–25] and IR [9, 14, 15] wavelengths, for OH measurements in flames [1, 2, 4, 5, 9–13], engines [3, 6, 7] and shock tubes [16–25]. Among these various OH diagnostic methods, UV-laser absorption spectroscopy is particularly useful as it can provide sensitive, quantitative, and time-resolved measurement of OH concentration.

A comprehensive survey of the OH absorption spectrum suggests that the strongest OH transitions at combustion-relevant temperatures are within the  $A^2\Sigma - X^2\Pi(0,0)$  rovibronic band in the UV (see Fig. 1) (according to HITRAN

2016 [26], the strongest IR transition is at least two orders of magnitude weaker). Several transitions in this band have been previously explored for sensitive OH detection [26–29], of which the  $R_1(5)$  transition particularly merits mention. Although not the strongest transition in the  $A - X(0,0)$  band,  $R_1(5)$  has historically been used for many quantitative measurements of OH in combustion research (e.g., [18, 19, 22–25]) due to its relative ease of access with frequency-doubled dye lasers, especially when stronger OH transitions were beyond conventional laser tuning ranges.

Very recently, advances in solid-state laser technologies have provided alternative UV light sources and enabled access to other OH transitions, including the strongest ones at combustion-relevant temperatures in the entire  $A - X(0,0)$  band:  $Q_1(4)$  at 308.42 nm,  $Q_1(5)$  at 308.61 nm, and  $Q_1(6)$  at 308.82 nm. As such, we were motivated to revisit the spectroscopy and to develop an optimized UV absorption diagnostic for OH. The current study focuses on the  $Q_1(5)$  transition, which is optimal for OH measurement over 1265–1880 K.

✉ Shengkai Wang  
sk.wang@stanford.edu

<sup>1</sup> High Temperature Gasdynamics Laboratory, Stanford University, Stanford, CA 94305, USA

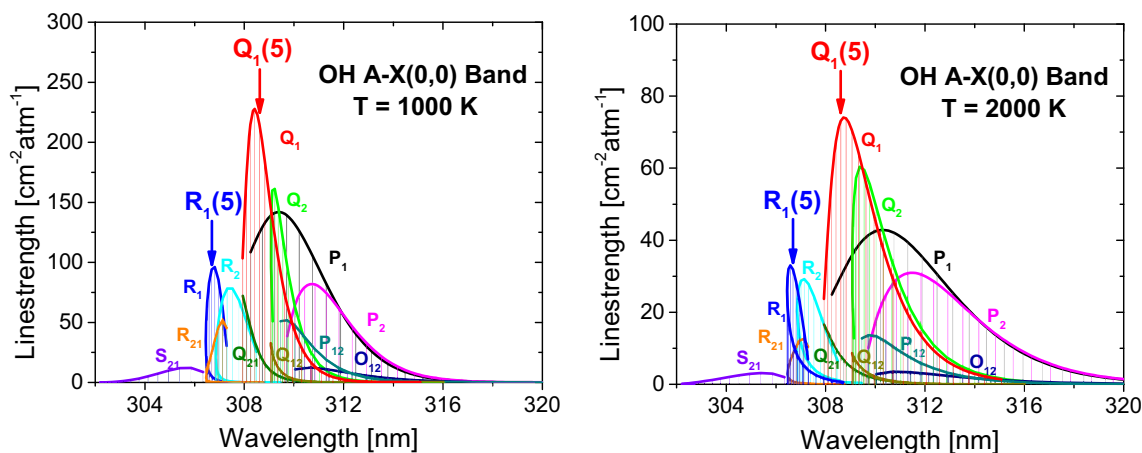


**Fig. 1** Simulated line strengths of OH  $A^2\Sigma - X^2\Pi$  (0,0) transitions at 1000 K (left) and 2000 K (right). Note that the  $Q_1(5)$  transition selected in the current study is one of the three strongest transitions

## 2 OH absorption spectroscopy

In a laser absorption measurement, the mole fraction ( $\chi$ ) of OH in a test gas mixture can be determined from the logarithmic attenuation of the laser intensity ( $-\ln(I/I_0)$ ), also known as absorbance ( $\alpha$ ), via the Beer–Lambert relation:  $\alpha = \chi kPL$ , where  $P$  is the total pressure of the test gas,  $L$  is the (assumed uniform) absorption pathlength, and  $k$  is the OH absorption coefficient, a spectroscopic parameter that is dependent on temperature, pressure, and wavelength. The current study targeted a distinctive and isolated absorption transition of OH for which  $k$  could be interpreted in a relatively simple manner:  $k = S(T)\varphi(\nu, T, P)$ , with  $S$  being the integrated line strength (in units of  $\text{cm}^{-2} \text{atm}^{-1}$ ) and  $\varphi$  being the spectral lineshape function (in cm units). The temperature dependence of the line strength  $S$ , relative to a reference temperature of choice,  $T_0$ , is given by

$$\frac{S(T)}{S(T_0)} = \frac{Q(T_0)}{Q(T)} \left(\frac{T_0}{T}\right) \exp\left[-\frac{hcE''}{k} \left(\frac{1}{T} - \frac{1}{T_0}\right)\right] \left[1 - \exp\left(-\frac{hcv_0}{kT}\right)\right] \left[1 - \exp\left(-\frac{hcv_0}{kT_0}\right)\right]^{-1}, \tag{1}$$

where  $Q$  is the OH partition function,  $E''$  and  $\nu_0$  are the lower-state energy and the line-center frequency of the OH absorption transition, and  $h$ ,  $c$ ,  $k$  are Planck’s constant, the speed of light, and Boltzmann’s constant, respectively. Regarding the  $Q_1(5)$  transition explored in the current study, values of  $E''$  and  $\nu_0$  have been determined with high accuracy in the work of Goldman and Gills [30]:  $E'' = 544.809 \text{ cm}^{-1}$  and  $\nu_0 = 32403.405 \text{ cm}^{-1}$ .  $Q(T)$  has also been tabulated by Goldman and Gills, with a minor correction for anharmonic oscillator effects discussed later by Goldman [32]. Over 1000–4000 K, in the current study,  $Q(T)$  is fitted with

the following polynomial expression, which is valid over 1000–4000 K within  $\pm 0.3\%$  error:

$$Q(T) = 11.367 + 1.194 \times 10^{-1} T/K + 1.364 \times 10^{-5} (T/K)^2 + 1.600 \times 10^{-9} (T/K)^3. \tag{2}$$

To place absorption measurements on an absolute basis, one needs to know the precise value of  $S$  at the reference temperature  $T_0$ . However,  $S(T_0)$  was conventionally calculated from the Einstein A coefficient, which was typically determined on a relative basis (e.g., Chidsey and Crosley [33]) with respect to a particular vibrational/rotational state (e.g., the  $N' = 0, v' = 0$  state whose natural lifetime was measured by German [34]). The current study is hence motivated to provide a direct measurement of the line strength  $S$  for the OH  $Q_1(5)$  transition, particularly at a temperature representative of combustion situations.

Another prerequisite for quantitative and accurate measurement of OH concentration is a detailed understanding of the spectral lineshape,  $\varphi$ . Under the current experimental conditions, the lineshape is affected simultaneously by contributions from Doppler and collisional/pressure-broadening and can be described by a Voigt profile:  $\phi = 2\sqrt{\ln 2} V(x, a) / \sqrt{\pi} \Delta\nu_D$ , where  $\Delta\nu_D = 5.629 \times 10^{-3} (T/K)^{1/2} \text{ cm}^{-1}$  is the Doppler linewidth (FWHM) of the  $Q_1(5)$  transition,  $V(x, a)$  is the normalized Voigt function,  $x = 2\sqrt{\ln 2} (\nu - \nu_0 - \delta \cdot P) / \Delta\nu_D$  is the

normalized frequency detuning relative to line center, and  $a = \sqrt{\ln 2} \Delta\nu_C / \Delta\nu_D$  is a measure of the relative scale of the collisional vs. the Doppler linewidth. The collisional linewidth  $\Delta\nu_C$  is proportional to the pressure of the collisional partner of OH, i.e.,  $\Delta\nu_C = 2\gamma(T) \cdot P$ . To accurately model the lineshape of the OH  $Q_1(5)$  transition at various temperatures and pressures, it is necessary to characterize the lineshape parameters  $\delta$  (the pressure-shift coefficient) and  $2\gamma$ , which is another objective of the current study.

### 3 Experimental method

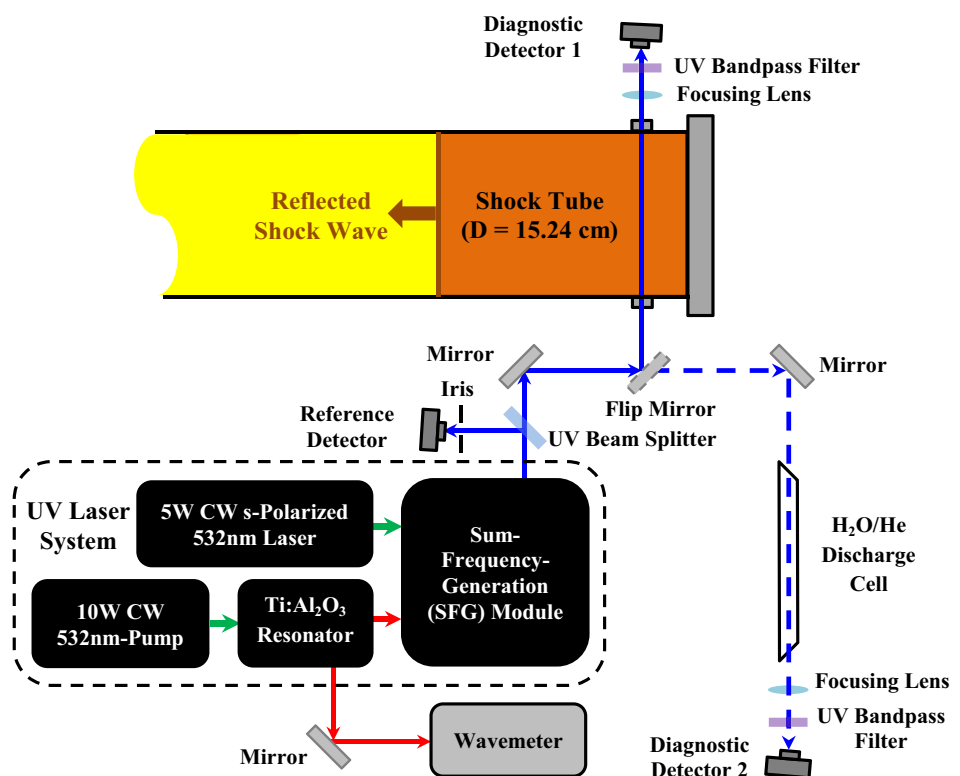
High-temperature OH absorption measurements were conducted in a 15.24-cm diameter high-purity shock tube utilizing a state-of-the-art solid-state UV laser, as illustrated in Fig. 2. Known concentrations of OH radical were generated by shock-heating a 0.1% H<sub>2</sub>/0.1% O<sub>2</sub>/Ar mixture. The mixture was manometrically prepared in a 40-L mixing tank using a double-dilution procedure described in our earlier work [35]. Between shock experiments, the shock tube and mixing assembly were routinely evacuated to less than 6  $\mu$ torr to remove possible residual impurities. Further details about this Stanford shock tube facility have been documented in our previous study [36] and are not repeated here.

The UV-laser diagnostic was accessed through a pair of windows located 2 cm away from the shock tube endwall. To access the OH  $Q_1(5)$  transition near 308.61 nm, the current

diagnostic employed a sum-frequency-generation (SFG) solid-state laser system, which consisted of four different components: a 10-W CW 532-nm pump laser (Lighthouse Photonics Sprout™), a Ti:sapphire resonator (M-Squared™ SolsTiS), a frequency- and polarization-stabilized CW 532-nm laser (Coherent Verdi™ V-5, with a maximum power of 5.5 W), and a frequency mixing/SFG module (M-Squared™ ECD-X). The Ti:sapphire resonator was optically pumped by the 10-W 532-nm laser to generate about 2 W of laser radiation at 734.48 nm, which was fed into the SFG module together with the stabilized 532-nm laser for frequency mixing, and the resulting 308.61-nm UV output (up to 300 mW achievable, but set to about 10 mW in the current study to avoid detector damage) was directed to the shock tube for OH measurement.

Wavelength tuning of the UV laser was achieved by adjusting the output wavelength of the Ti:sapphire resonator using the M-Squared™ control software. While a rapid wavelength-scanning measurement strategy is still under development, this study adopted a fixed-wavelength direct-absorption strategy—the laser was tuned to a target wavelength and kept constant during each reflected shock wave experiment. The actual wavelength of the Ti:sapphire resonator output was monitored in real time with a Burleigh™ WA-1000 wavemeter, which had a spectral resolution of 0.01 cm<sup>-1</sup>. Both the Ti:sapphire resonator and the SFG module were stabilized with active feedback control to minimize wavelength and intensity drifts (less than  $\pm 0.01$  cm<sup>-1</sup> within

**Fig. 2** Schematic of the experimental setup used in the current study



30 min and less than  $\pm 0.5\%$  within 100 s, respectively). Using a flip mirror, the UV laser was also guided through a low-pressure ( $< 10$  torr) flowing  $\text{H}_2\text{O}/\text{He}$  microwave discharge cell. This microwave discharge served as a room-temperature OH source with negligible pressure-induced spectral shift and hence provided a good spectral reference for the OH line center.

Transmitted UV-laser intensities through the shock tube and the discharge cell were measured with Thorlabs<sup>TM</sup> PDA36A Si switchable-gain detectors (20 dB gain setting,  $f_{-3\text{dB}} = 1$  MHz). A UV beam splitter redirected part of the beam onto a bandwidth-matched reference detector whose signal was used to normalize the diagnostic detectors signals. This scheme, typically referred to as common-mode rejection, successfully reduced the laser intensity noise to less than  $\pm 0.1\%$ . To block the emission of the shock-heated gas or the microwave discharge, a set of UV bandpass filters (Newport<sup>TM</sup> FSR-UG5) were placed in front of the diagnostic detectors; similarly, an iris was placed in front of the reference detector to block background light. The detector signals were digitally sampled with a 14-bit data acquisition system (National Instruments<sup>TM</sup> PXIe-5122) at 100 MS/s for anti-aliasing, and low-pass-filtered to 1.25 MHz to reduce bit-noise and electronic noise. Note that 1.25 MHz was still higher than the detectors' bandwidth (1 MHz), so that the temporal resolution was never compromised.

## 4 Results and discussion

A direct comparison of OH absorption signals, measured at the peaks of the  $Q_1(5)$  and  $R_1(5)$  transitions in two nearly identical reflected shock experiments, is shown in Fig. 3. A

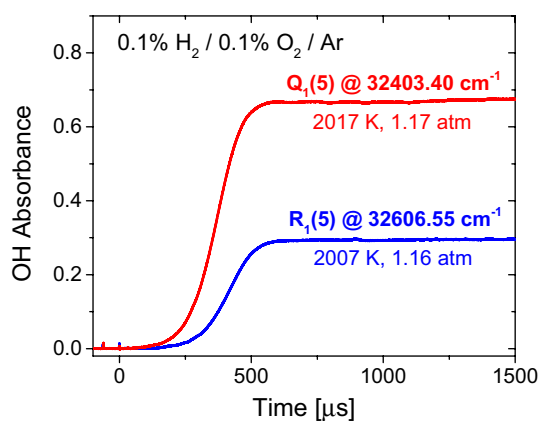


**Fig. 3** OH absorbance time histories measured at the  $Q_1(5)$  and  $R_1(5)$  peaks during shock tube oxidation experiments in a 1000 ppm  $\text{H}_2/1000$  ppm  $\text{O}_2/\text{Ar}$  mixture. Post-reflected-shock condition:  $T=2012 \pm 5$  K,  $P=1.16 \pm 0.01$  atm,  $\chi_{\text{OH,peak}} = 165 \pm 3$  ppm. Note that the  $Q_1(5)$  transition selected in the current study is more than 2.2 times the strength of our previously used  $R_1(5)$  transition

mixture of 0.1%  $\text{H}_2/0.1\%$   $\text{O}_2/\text{Ar}$  was shock-heated to temperatures of approximately 2010 K and pressures of 1.16 atm. OH was generated through the oxidation of hydrogen, and its concentration rapidly reached a plateau of 165 ppm. This value was determined from the  $R_1(5)$  measurement using OH absorption coefficient characterized in previous studies [29, 37], and was in excellent agreement (within  $\pm 3$  ppm difference) with predictions of several reaction models, such as Aramco 2.0 [38], USC Mech II [39] and the Li et al. model [40]. As evidenced, the current  $Q_1(5)$  diagnostic yielded a much stronger (a factor of  $2.24 \pm 0.08$ ) absorption signal compared to our previous  $R_1(5)$  diagnostic.

These experiments allowed for direct measurement of the OH absorption coefficient. Moreover, we have also mapped out the absorption lineshapes of the OH  $Q_1(5)$  transition by repeated reflected shock experiments at similar temperatures and pressures but with slight offsets in wavelength. Figure 4 shows the measured  $Q_1(5)$  lineshapes at  $T=2008$  K,  $P=1.16$  and 4.06 atm. Notably, the OH absorption spectrum became broader and slightly shifted to the low-frequency side at higher pressures. By fitting the measured lineshapes with Voigt profiles, we have determined the integrated line-strength ( $S$ ), the Ar-broadening ( $2\gamma_{\text{Ar}}$ ) and the Ar-shifting ( $\delta_{\text{Ar}}$ ) coefficients of the  $Q_1(5)$  transition at 2008 K, as shown in Table 1. A more sophisticated model of the OH absorption spectrum could incorporate speed-dependent lineshape [41] and collision-induced narrowing [42], however, according to the previous studies of Rea et al. [29] and Herbon [37], these effects were small (less than  $\pm 2\%$  deviation from the Voigt profile) at the current experimental conditions and hence were omitted in this study.

Similar values of  $2\gamma_{\text{Ar}}$  are observed between the  $Q_1(5)$  and  $R_1(5)$  transitions, which is expected due to the same lower-state rotational quantum number ( $J'' = 5.5$ ) shared by

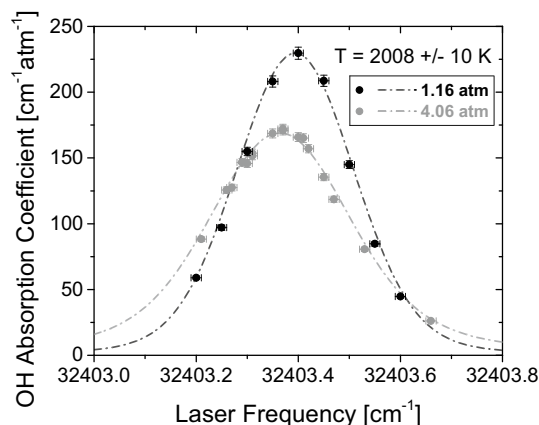


**Fig. 4** Spectral lineshapes of the OH  $Q_1(5)$  transition at  $T=2008$  K,  $P=1.16$  and 4.06 atm. Symbols: current data; lines: current Voigt fit. Error bars denote  $1-\sigma$  uncertainties in laser frequency (horizontal  $\pm 0.01$   $\text{cm}^{-1}$ ) and OH absorption coefficient (vertical  $\pm 2\%$ )

**Table 1** Spectroscopic parameters of the OH  $Q_1(5)$  vs.  $R_1(5)$  transitions at  $T=2008$  K

	$\nu_0$ (cm <sup>-1</sup> )	$E''$ (cm <sup>-1</sup> )	$S$ (cm <sup>-2</sup> atm <sup>-1</sup> )	$2\gamma_{Ar}$ (cm <sup>-1</sup> atm <sup>-1</sup> )	$\delta_{Ar}$ (cm <sup>-1</sup> atm <sup>-1</sup> )
$Q_1(5)$	32403.405 <sup>a</sup>	544.809 <sup>a</sup>	$71 \pm 2.5^b$	$0.034 \pm 0.005^b$	$-0.010 \pm 0.0025^b$
$R_1(5)$	32606.557 <sup>a</sup>	543.575 <sup>a</sup>	31.65 <sup>a</sup>	$0.032 \pm 0.003^c$	$-0.0100 \pm 0.0002^d$

Values obtained from <sup>a</sup>Golden and Gillis [30]; <sup>b</sup>current study; <sup>c</sup>Rea et al. [29]; <sup>d</sup>Herbon [37]

these two transitions. The similarity in  $\delta_{Ar}$ , however, is perhaps a coincidence [cross-over of  $Q_1(J'')$  and  $R_1(J'')$ ], as the  $J''$ -dependence of  $\delta_{Ar}$  is generally different for each branch [37]. The uncertainties in current determinations of  $2\gamma_{Ar}$  and  $\delta_{Ar}$  are dominated by the spectral resolution of the fixed-wavelength measurements. Future experiments are planned to improve the accuracy of these measurements using rapid wavelength scanning.

The temperature dependence of the  $Q_1(5)$  linestrength  $S$  was determined from Eq. 1. To simplify the mathematical expression, the results have been fitted to the following form:

$$S(T) = \exp[6.81 - 1.71 \times 10^{-3}T/K + 2.59 \times 10^{-7}(T/K)^2 - 2.00 \times 10^{-11}(T/K)^3] \text{ cm}^{-2} \text{ atm}^{-1}. \quad (3)$$

The overall  $1 - \sigma$  uncertainty in this expression, including both measurement uncertainty and fitting error, is estimated to be less than  $\pm 4\%$ . As for  $2\gamma_{Ar}$  and  $\delta_{Ar}$ , the previous studies of Rea et al. [29] and Herbon [37] suggested that for the OH transitions in the  $A - X(0,0)$  band, they generally follow a  $T^{-0.8}$  dependence. Hence to the first-order approximation, and for the temperature range of current interest (about 1200–3000 K), we can express the Ar-broadening and Ar-shifting parameters of the  $Q_1(5)$  transition as follows:

$$2\gamma_{Ar}(T) = 0.034 \times (2000 \text{ K} / T)^{0.8} \text{ cm}^{-1} \text{ atm}^{-1}, \quad (4)$$

$$\delta_{Ar}(T) = -0.010 \times (2000 \text{ K} / T)^{0.8} \text{ cm}^{-1} \text{ atm}^{-1}. \quad (5)$$

Equations 3–5 provide a complete description for the OH absorption coefficient at  $Q_1(5)$ . To validate this spectroscopic model we directly measured the absorption coefficient and compared these data to the calculated values, as illustrated in Fig. 5. Excellent agreement is seen between the current measurement and model.

The following expression is a numerical fit for the OH absorption coefficient at  $32403.40 \text{ cm}^{-1}$  near the  $Q_1(5)$  line-center:

$$k = \exp(8.622 - 1.852T_r - 0.4328P_r + 0.1786T_r^2 + 0.1994T_rP_r + 0.0081P_r^2 - 0.0040T_r^3 - 0.0259T_r^2P_r - 0.0028T_rP_r^2 + 0.0002P_r^3) \text{ cm}^{-1} \text{ atm}^{-1}, \quad (6)$$

where  $T_r = T/1000$  K and  $P_r = P/1$  atm are the reduced/non-dimensional temperatures and pressures. This expression

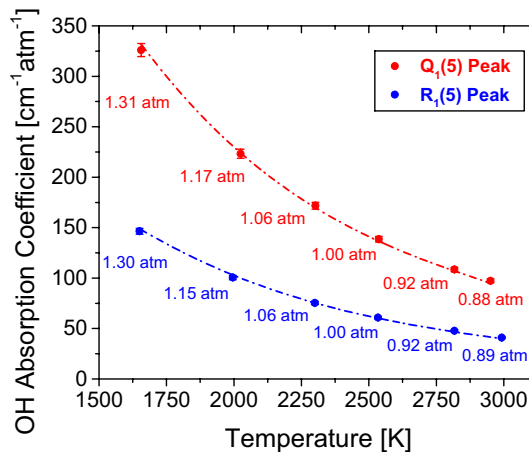


**Fig. 5** Peak OH absorption coefficients of  $Q_1(5)$  and  $R_1(5)$  at different temperatures (and pressures). Symbols: direct measurements. Lines: calculations based on the spectroscopic parameters listed above

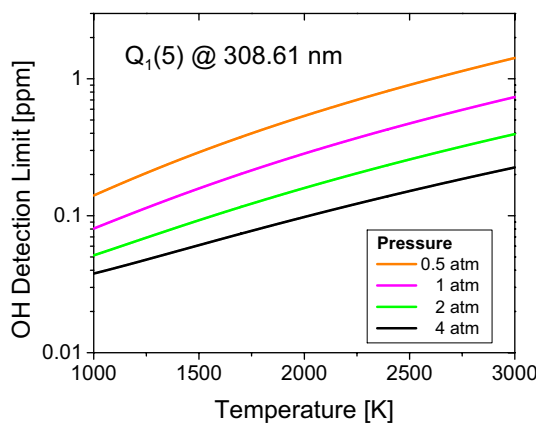


**Fig. 6** Projected  $1 - \sigma$  detection limit of the current OH diagnostic as a function of  $T$  and  $P$ . Assuming an optical pathlength of 15 cm and a minimum detectable absorption of 0.1%

should be valid over 1000–4000 K and 0.5–4 atm, with an estimated  $1 - \sigma$  overall uncertainty of  $\pm 5\%$ . Under the typical pathlength ( $\sim 15$  cm) and minimum detectable absorbance ( $1 \times 10^{-3}$ ) of Stanford shock tube facilities, sub-ppm-level OH detectivity is easily achievable with the current diagnostic (see Fig. 6).



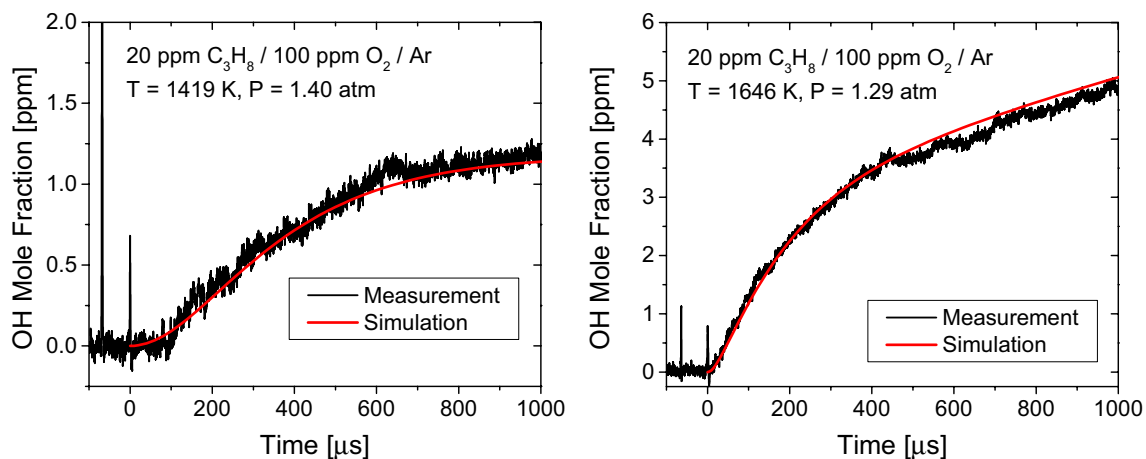


**Fig. 7** Example OH time histories measured during Ar-diluted stoichiometric oxidation of 20 ppm  $C_3H_8$ . Left:  $T = 1419$  K,  $P = 1.40$  atm. Right:  $T = 1646$  K,  $P = 1.29$  atm. In both cases, the  $1 - \sigma$

detection limit of OH was less than 0.15 ppm. Excellent agreement is observed between the measurements and kinetics simulations performed using the Aramco 2.0 mechanism [38]

## 5 Example application

This new OH diagnostic is intended for use in future kinetics experiments, but here, we report on initial tests to demonstrate and validate its use in shock tube oxidation of dilute  $C_3H_8$  mixtures. Exhibited in Fig. 7 are two example OH measurements at  $T = 1419$  K and 1646 K, respectively. Even at these extremely low OH concentrations, signal-to-noise ratios of 10 or higher were readily achieved. Shown in comparison with the current measurements are kinetics simulations using the Aramco 2.0 mechanism [38], which is seen to be in excellent agreement with the measurements.

## 6 Conclusions and future work

In this study, we have developed a high-sensitivity diagnostic for OH using laser absorption at 308.61 nm, aimed particularly at shock tube applications. This new diagnostic utilizes the  $Q_1(5)$  transition of the OH  $A - X(0,0)$  band, one of the strongest OH absorption transitions at elevated temperatures, and has improved the OH detection sensitivity relative to the previous  $R_1(5)$  diagnostic by a factor of  $2.24 \pm 0.08$ . The OH absorption coefficient at the  $Q_1(5)$  transition was measured behind reflected shock waves at various temperatures, pressures and wavelengths. From these measurements, we have also determined the linestrength and the Ar-broadening and -shift coefficients of this transition.

We have demonstrated the unprecedented sensitivity of this new diagnostic in highly-diluted  $C_3H_8$  oxidation experiments, where a  $1 - \sigma$  detection limit of less than 0.15 ppm OH was achieved. Future extensions of the current work will involve applications of this high-sensitivity OH diagnostic to shock tube kinetics studies and also will aim to address other

spectroscopic questions. For example, we are interested in investigating use of the  $Q_1(4)$  and  $Q_1(6)$  transitions that are slightly stronger (by up to 15% and 5%) than  $Q_1(5)$  over the temperature ranges of 800–1250 and 1900–2650 K, respectively. We would also like to explore possibilities of rapid wavelength scanning, with hopes of obtaining more accurate determinations of lineshape and shift coefficients.

**Acknowledgements** This work was supported by the Air Force Office of Scientific Research through AFOSR Grant No. FA9550-14-1-0235, with Dr. Chiping Li as contract monitor.

## References

1. G. Kychakoff, R.D. Howe, R.K. Hanson, J.C. McDaniel, Quantitative visualization of combustion species in a plane. *Appl. Opt.* **21**, 3225–3227 (1982)
2. M.J. Dyer, D.R. Crosley, Two-dimensional imaging of OH laser-induced fluorescence in a flame. *Opt. Lett.* **7**, 382–384 (1982)
3. R. Suntz, H. Becker, P. Monkhouse, J. Wolfrum, Two-dimensional visualization of the flame front in an internal combustion engine by laser-induced fluorescence of OH radicals. *Appl. Phys. B.* **47**, 287–293 (1988)
4. C.F. Kaminski, J. Hult, M. Aldén, High repetition rate planar laser induced fluorescence of OH in a turbulent non-premixed flame. *Appl. Phys. B.* **68**, 757–760 (1999)
5. K. Kohse-Höinghaus, U. Meier, B. Attal-Trétout, Laser-induced fluorescence study of OH in flat flames of 1–10 bar compared with resonance CARS experiments. *Appl. Opt.* **29**, 1560–1569 (1990)
6. P. Andresen, G. Meijer, H. Schlüter, H. Voges, A. Koch, W. Hentschel, W. Oppermann, E. Rothe, Fluorescence imaging inside an internal combustion engine using tunable excimer lasers. *Appl. Opt.* **29**, 2392–2404 (1990)
7. S. Singh, M.P. Musculus, R.D. Reitz, Mixing and flame structures inferred from OH-PLIF for conventional and low-temperature diesel engine combustion. *Combust. Flame.* **156**, 1898–1908 (2009)
8. A.G. Gaydon, *The Spectroscopy of Flames* (2nd edn.) (Wiley, New York, 1974)

9. J.P. Maillard, J. Chauville, A.W. Mantz, High-resolution emission spectrum of OH in an oxyacetylene flame from 3.7 to 0.9  $\mu\text{m}$ . *J. Mol. Spectrosc.* **63**, 120–141 (1976)
10. J. Luque, J.B. Jeffries, G.P. Smith, D.R. Crosley, K.T. Walsh, M.B. Long, M.D. Smooke, CH(A-X) and OH(A-X) optical emission in an axisymmetric laminar diffusion flame. *Combust. Flame.* **122**, 172–175 (2000)
11. J. Kojima, Y. Ikeda, T. Nakajima, Spatially resolved measurement of OH\*, CH\*, and C2\* chemiluminescence in the reaction zone of laminar methane/air premixed flames. *Proc. Combust. Inst.* **28**, 1757–1764 (2000)
12. B. Higgins, M.Q. McQuay, F. Lacas, J.C. Rolon, N. Darabiha, S. Candel, Systematic measurements of OH chemiluminescence for fuel-lean, high-pressure, premixed, laminar flames. *Fuel.* **80**, 67–74 (2001)
13. M. De Leo, A. Saveliev, L.A. Kennedy, S.A. Zelepouga, OH and CH luminescence in opposed flow methane oxy-flames. *Combust. Flame.* **149**, 435–447 (2007)
14. B.L. Upschulte, D.M. Sonnenfroh, M.G. Allen, Measurements of CO, CO<sub>2</sub>, OH, and H<sub>2</sub>O in room-temperature and combustion gases by use of a broadly current-tuned multisection InGaAsP diode laser. *Appl. Opt.* **38**, 1506–1512 (1999)
15. T. Aizawa, Diode-laser wavelength-modulation absorption spectroscopy for quantitative in situ measurements of temperature and OH radical concentration in combustion gases. *Appl. Opt.* **40**, 4894–4903 (2001)
16. R.K. Hanson, S. Salimian, G. Kychakoff, R.A. Booman, Shock-tube absorption measurements of OH using a remotely located dye laser. *Appl. Opt.* **22**, 641–643 (1983)
17. E.C. Rea, S. Salimian, R.K. Hanson, Rapid-tuning frequency-doubled ring dye laser for high resolution absorption spectroscopy in shock-heated gases. *Appl. Opt.* **23**, 1691–1694 (1984)
18. M.A. Oehlschlaeger, D.F. Davidson, J.T. Herbon, R.K. Hanson, Shock tube measurements of branched alkane ignition times and OH concentration time histories. *Int. J. Chem. Kinet.* **36**, 67–78 (2004)
19. V. Vasudevan, D.F. Davidson, R.K. Hanson, Shock tube measurements of toluene ignition times and OH concentration time histories. *Proc. Combust. Inst.* **30**, 1155–1163 (2005)
20. S.S. Vasu, D.F. Davidson, Z. Hong, V. Vasudevan, R.K. Hanson, *n*-Dodecane oxidation at high-pressures: Measurements of ignition delay times and OH concentration time-histories. *Proc. Combust. Inst.* **32**, 173–180 (2009)
21. R. Sivaramakrishnan, J.V. Michael, Rate constants for OH with selected large alkanes: shock-tube measurements and an improved group scheme. *J. Phys. Chem. A.* **113**, 5047–5060 (2009)
22. J. Badra, A.E. Elwardany, F. Khaled, S.S. Vasu, A. Farooq, A shock tube and laser absorption study of ignition delay times and OH reaction rates of ketones: 2-Butanone and 3-buten-2-one. *Combust. Flame.* **161**, 725–734 (2014)
23. J. Badra, A. Elwardany, A. Farooq, Shock tube measurements of the rate constants for seven large alkanes + OH. *Proc. Combust. Inst.* **35**, 189–196 (2015)
24. S. Wang, D.F. Davidson, R.K. Hanson, High temperature measurements for the rate constants of C1–C4 aldehydes with OH in a shock tube. *Proc. Combust. Inst.* **35**, 473–480 (2015)
25. S. Wang, D.F. Davidson, R.K. Hanson, Rate constants of long, branched, and unsaturated aldehydes with OH at elevated temperatures. *Proc. Combust. Inst.* **36**, 151–160 (2017)
26. I.E. Gordon, L.S. Rothman, C. Hill, R.V. Kochanov, Y. Tan, P.F. Bernath, M. Birk, V. Boudon, The HITRAN2016 molecular spectroscopic database. *J. Quant. Spectrosc. Radiat. Transfer.* (2017). <https://doi.org/10.1016/j.jqsrt.2017.06.038> (in press)
27. D.F. Davidson, M. Roehrig, E.L. Petersen, M.D. Di Rosa, R.K. Hanson, Measurements of the OH AX (0, 0) 306 nm Absorption Bandhead at 60 atm and 1735 K. *J. Quant. Spectrosc. Radiat. Transfer.* **55**, 755–762 (1996)
28. A.Y. Chang, E.C. Rea, R.K. Hanson, Temperature measurements in shock tubes using a laser-based absorption technique. *Appl. Opt.* **26**, 885–891 (1987)
29. E.C. Rea, A.Y. Chang, R.K. Hanson, Shock-tube study of pressure broadening of the  $A^2\Sigma^+ - X^2\Pi$  (0, 0) band of OH by Ar and N<sub>2</sub>. *J. Quant. Spectrosc. Radiat. Transfer.* **37**, 117–127 (1987)
30. A. Goldman, J.R. Gillis, Spectral line parameters for the  $A^2\Sigma - X^2\Pi$  (0, 0) band of OH for atmospheric and high temperatures. *J. Quant. Spectrosc. Radiat. Transfer.* **25**, 111–135 (1981)
31. J. Luque, D.R. Crosley, *LIFBASE: Database and Spectral Simulation Program (Version 1.5)*, SRI International Report MP 99-009 (1999)
32. A. Goldman, Line parameters for the atmospheric band system of OH. *Appl. Opt.* **21**, 2100–2102 (1982)
33. I.L. Chidsey, D.R. Crosley, Calculated rotational transition probabilities for the A – X system of OH. *J. Quant. Spectrosc. Radiat. Transfer.* **23**, 187–199 (1980)
34. K.R. German, Direct measurement of the radiative lifetimes of the  $A^2\Sigma+(V'' = 0)$  states of OH and OD. *J. Chem. Phys.* **62**, 2584–2587 (1975)
35. S. Wang, E.E. Dames, D.F. Davidson, R.K. Hanson, Reaction rate constant of CH<sub>2</sub>O + H = HCO + H<sub>2</sub> revisited: A combined study of direct shock tube measurement and transition state theory calculation." *J. Phys. Chem. A.* **118**, 10201–10209 (2014)
36. S. Wang, K. Sun, D.F. Davidson, J.B. Jeffries, R.K. Hanson, Shock-tube measurement of acetone dissociation using cavity-enhanced absorption spectroscopy of CO. *J. Phys. Chem. A.* **119**, 7257–7262 (2015)
37. J.T. Herbon: Shock tube measurements of CH<sub>3</sub> + O<sub>2</sub> kinetics and the heat of formation of the OH radical, (Ph.D. Dissertation, Stanford University, 2004)
38. Y. Li, C.W. Zhou, K.P. Somers, K. Zhang, H.J. Curran, The oxidation of 2-butene: A high pressure ignition delay, kinetic modeling study and reactivity comparison with isobutene and 1-butene. *Proc. Combust. Inst.* **36**, 403–411 (2017)
39. H. Wang, X. You, A.V. Joshi, S.G. Davis, A. Laskin, F. Egol-fopoulos, C.K. Law, USC Mech version II. [http://ignis.usc.edu/USC\\_Mech\\_II.htm](http://ignis.usc.edu/USC_Mech_II.htm) (2007)
40. J. Li, Z. Zhao, A. Kazakov, F.L. Dryer, An updated comprehensive kinetic model of hydrogen combustion. *Int. J. Chem. Kinet.* **36**, 566–575 (2004)
41. P.R. Berman, Speed-dependent collisional width and shift parameters in spectral profiles. *J. Quant. Spectrosc. Radiat. Transfer.* **12**, 1331–1342 (1972)
42. P.L. Varghese, R.K. Hanson, Collisional narrowing effects on spectral line shapes measured at high resolution. *Appl. Opt.* **23**, 2376–2385 (1984)